



저작자표시-비영리-변경금지 2.0 대한민국

이용자는 아래의 조건을 따르는 경우에 한하여 자유롭게

- 이 저작물을 복제, 배포, 전송, 전시, 공연 및 방송할 수 있습니다.

다음과 같은 조건을 따라야 합니다:



저작자표시. 귀하는 원저작자를 표시하여야 합니다.



비영리. 귀하는 이 저작물을 영리 목적으로 이용할 수 없습니다.



변경금지. 귀하는 이 저작물을 개작, 변형 또는 가공할 수 없습니다.

- 귀하는, 이 저작물의 재이용이나 배포의 경우, 이 저작물에 적용된 이용허락조건을 명확하게 나타내어야 합니다.
- 저작권자로부터 별도의 허가를 받으면 이러한 조건들은 적용되지 않습니다.

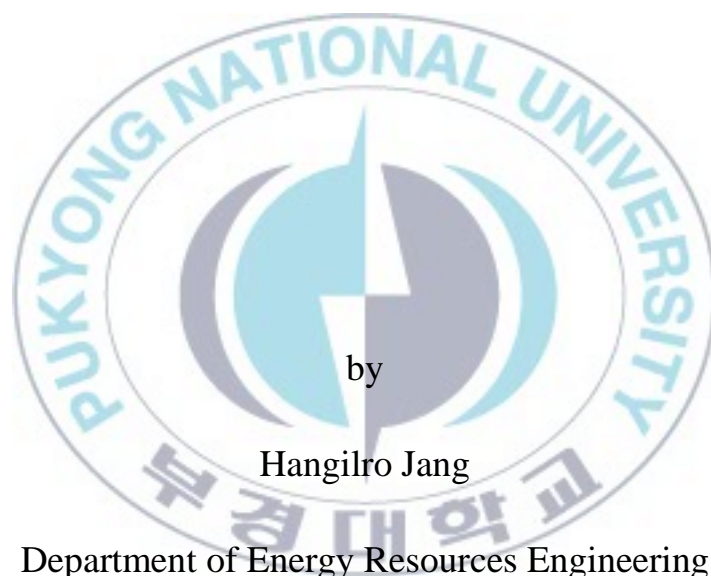
저작권법에 따른 이용자의 권리는 위의 내용에 의하여 영향을 받지 않습니다.

이것은 [이용허락규약\(Legal Code\)](#)을 이해하기 쉽게 요약한 것입니다.

[Disclaimer](#)

Thesis for the Degree of Master of Engineering

A study on the modeling of marine
controlled-source electromagnetic methods
for offshore resources



by

Hangilro Jang

Department of Energy Resources Engineering

The Graduate School

Pukyong National University

February 2013

A study on the modeling of marine
controlled-source electromagnetic methods
for offshore resources

(해양자원탐사를 위한 인공송신원
전자탐사법의 모델링 연구)



Advisor: Prof. Hee Joon Kim

by
Hangilro Jang

A thesis submitted in partial fulfillment of the requirements
for the degree of

Master of Engineering

in Department of Energy Resources Engineering, The Graduate School,
Pukyong National University

February 2013

A study on the modeling of marine
controlled-source electromagnetic methods
for offshore resources

A dissertation
by
Hangilro Jang



Approved by:

(Chairman) Jeong-Gi Um

(Member) Yo Soon Choi

(Member) Hee Joon Kim

February 2013

A study on the modeling of marine controlled-source electromagnetic methods for offshore resources

Hangilro Jang

Department of Energy Resources Engineering, The Graduate School,
Pukyong National University

Abstract

A frequency-domain, marine controlled-source electromagnetic (CSEM) method has been applied successfully in deep water areas for detecting hydrocarbon (HC) reservoirs. However, a typical technique with horizontal transmitters and receivers requires large source-receiver separations with respect to the target depth. A time-domain EM system with vertical transmitters and receivers can be an alternative because vertical electric fields are sensitive to deep resistive layers. Computer programs have been developed to evaluate EM responses for a one-dimensional (1-D) model with multiple source and receiver dipoles that are finite in length in both frequency- and time-domain. Using the frequency-domain code, we conducted sensitivity analysis of marine CSEM methods to a gas-hydrate layer in the shallow section. In this study we used a normalized amplitude and amplitude difference of EM fields simultaneously in determining the detection capability of the hydrate layer. The field amplitude must be normalized by the one for the corresponding background model without the hydrate layer. The normalized amplitude can be numerically large, but if the field amplitude is smaller than the threshold, it would be misleading and therefore is useless. From these numerical experiments, we found that there are plenty of useful offset ranges and frequencies where amplitude difference is large enough to detect the target layer. Furthermore, an effect of air waves is almost absent in amplitude

difference. With the use of time-domain code, we calculated step-off responses for 1-D HC reservoir models. Although the vertical electric field has much smaller amplitude of signal than the horizontal field, vertical currents resulting from a vertical transmitter are sensitive to resistive layers. The modeling shows a significant difference between step-off responses of HC- and water-filled reservoirs, and the contrast can be recognized at late times at relatively short offsets. A maximum contrast occurs at more than 4 s, being delayed with the depth of the HC layer.

Keywords: marine CSEM, gas hydrate, normalized amplitude, amplitude difference, air wave, hydrocarbon, step-off response, vertical transmitter



Contents

Abstract	i
List of figures	v
Chapter 1. Introduction	1
1.1. Background and motivation	1
1.2. Thesis overview	3
Chapter 2. Methods	4
2.1. Maxwell's equation	4
2.2. Extension of EM1D	5
2.3. Time-domain responses	6
Chapter 3. Marine CSEM sounding for detecting a gas-hydrate layer in the shallow seabed	9
3.1. Marine CSEM sounding	9
3.2. A Gas-hydrate model	11
3.3. Effect of seawater thickness	12
3.4. Effect of source dipole length	13
3.5. Comparison of electric and magnetic fields	14
3.6. Comparison of in-line and broadside arrays	15
3.7. Effect of source altitude	18
3.8. Effect of overburden thickness	19
Chapter 4. Step-off, vertical EM responses of a deep resistivity layer buried in marine sediments	20
4.1. Canonical reservoir model	20
4.2. Comparison of electric and magnetic fields	21
4.3. Effect of source-receiver distance	22

4.4. Effect of seawater thickness	25
4.5. Effect of overburden thickness	26
4.6. Effect of source dipole length	27
Chapter 5. Discussion and conclusions	29
References	33
Appendix	38
초 록	41
감사의 글	43



List of figures

Fig. 2.1. Normalized step-off responses at the surface of the homogeneous half-space. Solid lines indicate the analytic solution and dots are numerical results from a digital filter.

Fig. 3.1. An electric dipole transmitter is towed above the seafloor (~100 m) and an alternating EM field is transmitted along the antenna, which can be 100 – 300 m long. Seafloor receivers record electric fields (and magnetic fields) from the transmitter. BSR = bottom simulating reflector; GHSZ = gas hydrate stability zone (After Weitemeyer et al., 2006).

Fig. 3.2. 1-D marine CSEM model with variable depth to a resistive hydrate layer, and source length and altitude above the seafloor. EM fields are calculated for the model as a function of the transmitter-receiver separation and frequency.

Fig. 3.3 Normalized amplitude (in color shade) and amplitude difference (in line contour, $VA^{-1}m^{-2}$) in radial mode for the hydrate model in Fig. 3.2. The hydrate layer is buried at a depth of 50 m. The source dipole length is 100 m and its altitude is 100 m above the seafloor.

Fig. 3.4. Same as in Fig. 3.3 except that the water depth is 2000 m.

Fig. 3.5. Same as in Fig. 3.3 except that the background model is excited by a point dipole source. Three source dipole lengths are considered: (a) 100 m, (b) 200 m, and (c) 300 m.

Fig. 3.6. Normalized amplitude (in color shade) and amplitude difference (in line contour) in magnetic fields ($\gamma A^{-1} m^{-1}$) for the hydrate model in Fig. 3.2. The hydrate layer is buried at a depth of 50 m. A 100 m-long dipole source is situated at 100 m above the seafloor.

Fig. 3.7. Normalized amplitude (in color shade) and amplitude difference (in line contour, $VA^{-1} m^{-2}$) in azimuthal mode for the hydrate model in Fig. 3.2. The hydrate layer is buried at a depth of 50 m. A 100 m-long dipole source is situated at 100 m above the seafloor.

Fig. 3.8. Normalized amplitude (in color shade) and amplitude difference (in line contour, $VA^{-1} m^{-2}$) in azimuthal mode for a model with a 50 m-thick hydrate layer. The hydrate layer is buried at a depth of 50 m. A 100 m-long dipole source is situated at 100 m above the seafloor.

Fig. 3.9. Normalized amplitude (in color shade) and amplitude difference (in line contour, $VA^{-1} m^{-2}$) for the hydrate model in Fig. 3.2. The hydrate layer is buried at a depth of 50 m. A 100 m-long dipole source is situated at 50 m (left) and 200 m (right) above the seafloor.

Fig. 3.10. Normalized amplitude (in color shade) and amplitude difference (in line contour, $VA^{-1} m^{-2}$) for the hydrate model in Fig. 3.2. The hydrate layer is buried at depths of 30 m (left) and 80 m (right). A 100 m-long dipole source is situated at 100 m above the seafloor.

Fig. 4.1. A 1-D offshore HC reservoir model.

Fig. 4.2. Vertical responses from a vertical source for the HC reservoir model (red line), and the background model (blue line), and the horizontal responses from a horizontal source for the HC reservoir model (brown

line) and the background model (green line). Dashed and solid lines indicate negative and positive values of the response, respectively. The bottom lines indicate the electric-field amplitudes for the HC reservoir model normalized by the responses of the background model. A 10 m-long receiver is located 500 m away from a 100 m-long transmitter at the seafloor with a water depth of 1000 m. The resistive HC layer is buried at 1000 m below the seafloor.

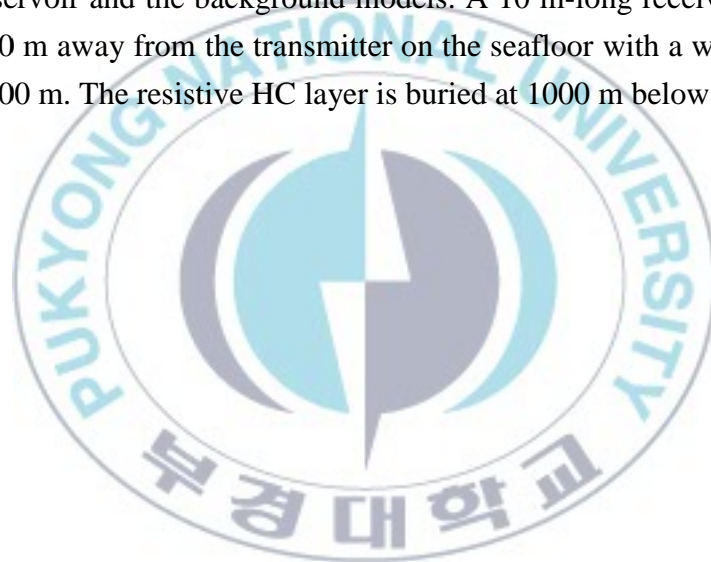
Fig. 4.3. Step-off magnetic-field responses for the HC reservoir model (red line) and the background model (blue line). The bottom gray line indicates the magnetic-field amplitude for the HC reservoir model normalized by the response of the background model. A horizontal magnetometer is located 500 m away from a 100 m-long transmitter at the seafloor with a water depth of 1000 m. The resistive HC layer is buried at 1000 m below the seafloor.

Fig. 4.4. Step-off responses for various offsets between the source and receiver over the HC reservoir model (solid lines) and the background model (dashed lines). The bottom lines indicate the ratios between the responses of the HC reservoir and the background models. A 100 m-long transmitter and 10 m-long receiver are located on the seafloor with a water depth of 1000 m. The resistive HC layer is buried at 1000 m below the seafloor.

Fig. 4.5. Step-off responses for various water depths over the HC reservoir model (solid lines) and the background model (dashed lines). The bottom lines indicate the ratios between the responses of the HC reservoir and the background models. A 100 m-long transmitter and 10 m-long receiver are located on the seafloor and the offset is 500 m. The resistive HC layer is buried at 1000 m below the seafloor.

Fig. 4.6. Step-off responses for various depths of the resistive HC layer over the HC reservoir model (solid lines) and the background model (dashed line). The bottom lines indicate the ratios between the responses of the HC reservoir and the background models. A 10 m-long receiver is located 500 m away from a 100 m-long transmitter on the seafloor with a water depth of 1000 m.

Fig. 4.7. Step-off responses for various source lengths over the HC reservoir model (solid lines) and the background model (dashed lines). The bottom lines indicate the ratios between the responses of the HC reservoir and the background models. A 10 m-long receiver is located 500 m away from the transmitter on the seafloor with a water depth of 1000 m. The resistive HC layer is buried at 1000 m below the seafloor.



Chapter 1. Introduction

1.1. Background and motivation

The great progress in computational and instrument has been made it possible to a controlled-source electromagnetic (CSEM) method for offshore exploration. In the early days, the marine CSEM method carried out to determine conductivity of oceanic lithosphere (Cox et al., 1986). Since, it began to be known that the marine CSEM method is very useful to detect a resistive medium such as hydrocarbon (HC) and gas-hydrate, the major oil companies have been showed great interests in the method. First successful commercial exploration in the Angola region has been accelerated the development of the method and recently has become an important exploration tool for the HC industry (Ellingsrud et al., 2002, Constable, 2010). Furthermore, Kang et al. (2012) showed the feasibility of the offshore CO₂ sequestration monitoring.

A gas hydrate deposit can be generally identified in a seismic section as a bottom simulating reflector (BSR) which is associated with the base of a hydrate stability zone (HSZ). This lower stratigraphic boundary is a transition zone between hydrate bearing sediments above it and free gas and water below it. The location of HSZ is temperature controlled and depends on the ambient geothermal gradient. The diffuse upper boundary is not as well marked so that the total mass of hydrate is not determined easily by seismic alone, and there is generally no seismic signature from within the hydrate volume.

Electrical resistivity of marine sediments is mainly controlled by the amount of seawater in the available pore space, the porosity. It is typically around 1 Ω -m just beneath the seafloor. Because hydrate itself is an electrical insulator and forms in the available pore space within HSZ replacing conductive pore fluid, electrical resistivity can rise significantly (Edwards,

1997; Weitemeyer et al., 2006). Electrical resistivity measurements made in well logs characterize a region containing hydrate as more resistive when compared to background sediments without hydrate. Needless to say, drilling is expensive and drilling into hydrates can be hazardous, destabilizing HSZ.

For gas hydrate characterization a short-offset time-domain electric dipole-dipole system was used in the Cascadia margin off the coast of Vancouver Island, British Columbia, Canada (Yuan and Edwards, 2000; Schwalenberg et al., 2005). In contrast, Weitemeyer et al. (2006) employed a frequency-domain CSEM method to detect gas hydrates at Hydrate Ridge, offshore Oregon.

The marine CSEM method is used in both frequency- and time-domain. A typical marine CSEM technique uses horizontal sources and receivers with in-line geometry. At greater ranges, EM energy that has leaked into the air and propagates back to the seafloor begins to dominate the CSEM signal. This airwave effect is a consequence of the absence of attenuation in the air and more significant in shallow water (e.g., Constable 2010). Experience from land EM suggests that the best approach to dealing with the airwave is by using time-domain, instead of frequency-domain methods (Weiss, 2007, Li and Constable, 2010).

Two different marine CSEM methods are available in time domain (Hunziker et al., 2011). The first method uses a horizontal source for a fast data acquisition (Chave et al., 1991, Ziolkowski, 2007). A processing scheme proposed by Ziolkowski (2007), for example, deconvolves the recorded signal with the source signal, a pseudo-random binary sequence, to recover the earth impulse response. In contrast, the second method uses a vertical source for minimizing an airwave effect (Edwards et al., 1985, Holten et al., 2009). Holten et al. (2009) used a source signal consisting of eight square pulses followed by silent periods, and the signal was stacked over these pulses to reduce noise. The recorded data at a vertical receiver due to a vertical source may have good resolution to resistive layers even at short offsets (Scholl and Edwards, 2007, Holten et al., 2009).

The difficulty when measuring vertical rather than horizontal electric fields is the small amplitude of the signal. The horizontal response from a horizontal source is 2–3 orders of magnitude stronger at late times than the vertical response from a vertical source (Chave and Cox 1982). This means that both source and receiver tilt angles must be kept very small (Hunziker et al., 2011), but it is difficult to achieve the verticality of sources and receivers. However, vertical sources have the advantage of not producing an airwave, because they generate a pure transverse magnetic (TM) mode field (Um and Alumbaugh 2007, Holten et al., 2009, Hunziker et al., 2011).

1.2. Thesis overview

The second chapter represents algorithms to comprehensive investigation of EM responses of a one-dimensional (1-D) layered earth with finite-length dipoles in both frequency- and time-domain. The time-domain responses can be obtained from a Fourier transform of frequency-domain responses which is mentioned above.

The third chapter shows sensitivity analysis of a shallow gas-hydrate layer in frequency-domain. In this chapter, normalized amplitude and amplitude difference are used simultaneously in determining the detection capability of the hydrate layer.

In the fourth chapter, vertical electromagnetic responses of a deep resistivity layer buried in marine sediments are calculated in time-domain. Effects of source-receiver distance, water thickness, overburden thickness and source length are investigated. A step-off source waveform is used and the ramp time is set to be negligibly small.

The concluding chapter briefly discusses and summarizes for the previous chapters. Then some possible ways for future research are proposed based on the work presented in this thesis.

Chapter 2. Methods

2.1. Maxwell's equation

The EM1D code for isotropic layered earth EM responses is based on general theory of analytic solution of the EM fields (Kim et al., 1997, Song et al., 2002). The computations consider the case where a dipole source is placed within one of several stratified layers with air body and earth half space at the top and bottom respectively of the stack of layers.

Assuming an $e^{i\omega t}$ time dependence, Maxwell's equations in frequency-domain is given by

$$\nabla \times \mathbf{E} + i\mu\omega\mathbf{H} = 0 \quad (1)$$

$$\nabla \times \mathbf{H} - (\sigma + i\varepsilon\omega)\mathbf{E} = 0 \quad (2)$$

where $\mu_0 = 4\pi \times 10^{-7}$ H/m, ω is the angular frequency, σ is the conductivity and ε is the dielectric permittivity. Upon taking the curl of each, we obtain the Helmholtz equations of electric and magnetic fields in the low-frequency limit

$$\nabla \times \nabla \times \mathbf{E} + i\mu\omega\sigma\mathbf{E} = 0 \quad (3)$$

$$\nabla \times \nabla \times \mathbf{H} + i\mu\omega\sigma\mathbf{H} = 0 \quad (4)$$

The analytic solution for the EM fields of a point source such as a electric dipole in the presence of layered earth can be simplified if the solution is developed in terms of transverse electric (TE) and TM modes.

Because changes in physical properties coincide with coordinate surfaces (planes of constant z) we can solve the boundary-value problem by converting the partial differential equation to an ordinary differential equation in z . This conversion takes the form of a Hankel or 2-D Fourier transform since the coordinate surfaces are infinite in extent in the x and y directions. The solution in Fourier transform space can be derived using the plane-wave impedance formulas for a layered earth. Then, the final solution obtained by inverse Fourier or Hankel transformation (Ward and Hohmann, 1987).

2.2 Extension of EM1D

The computer program EM1D has been modified to comprehensive investigation of EM responses of a 1-D layered earth in frequency domain (Lee et al., 2011). Source and receiver electric dipoles may now consist of multiple dipoles of finite-length with arbitrary polarizations.

In general, the source and the receiver are considered as a set of finite-length source dipoles and the receiver as a set of finite-length receiver dipoles. The resulting electric field may be obtained by numerically integrating along all the source and receiver dipoles. Symbolically, it can be written as

$$E_{\text{EM1D}-f} = \sum_{jr=1}^{NR} \sum_{j=1}^{NJ} w_{j,jr} l_{j,jr} \sum_{ir=1}^{NS} \sum_{i=1}^{NI} w_{i,ir} l_{i,ir} E_{\text{EM1D}}(r_{j,jr}, r_{i,ir}) \quad (5)$$

Here, NS is finite-length sources and NR is finite-length receivers. Each source and receiver is then divided into NI and NJ segments, respectively, short enough to be considered point dipoles. Coefficients $w_{i,ir}$ and $w_{j,jr}$ are the weights typically used for the numerical integration, and $l_{i,ir}$ and $l_{j,jr}$ are the lengths of the source and receiver segments. A trapezoidal rule is used for the weighting. The actual summation process involves one more step in addition to the above expression because an arbitrarily oriented dipole consists of three

Cartesian components, both for the source and the receiver.

To define a finite-length dipole in model domain, Cartesian coordinates of two end points of the dipole are used as input. The direction of current flow or the voltage measurements are dictated by the order of input of the end points. The accuracy of the numerical summation largely depends on how finely the given dipoles are divided. It depends on the source-receiver dipole separation and the frequency used, but only the dipole separation is considered under current development.

2.3. Time-domain responses

Transient EM responses, $e(t)$, can be obtained from a Fourier transform of frequency-domain responses, $E(\omega)$,

$$e(t) = \frac{1}{2\pi} \int_{-\infty}^{\infty} E(\omega) e^{i\omega t} d\omega, \quad (6)$$

The time-domain solution in equation (6) is evaluated by fast Fourier transform (FFT) for efficiency. Frequency-domain responses are first obtained for a selected number of frequencies, e.g., 10 logarithmically equidistance samples per decade, and then spline interpolated to get the FFT input. In the code developed in this study, one can choose from one of the four current waveforms: step-off, square, impulse, and INPUT (see Appendix). Ramp time is optional to the step-off or square waveform, and its shape is linear in time. The frequency-domain result is obtained from the code developed by Lee et al. (2011) to include multiple source and receiver dipoles that are finite in length.

The lowest (fundamental) frequency used in FFT is determined by the period (T) of a chosen waveform as $1/T$. The highest (Nyquist) frequency is not directly related to the waveform. To achieve minimally aliased and accurate time-domain results, one needs to get high enough frequency data and use them

in the inverse Fourier transform. Selection of the highest frequency limit can be safely done by making sure that the minimum source-receiver distance is more than 10 skin depths over which EM fields are expected to be sufficiently attenuated.

A horizontal step-off response of the inline electric field, $e_x(t)$, from a unit horizontal source dipole at the surface of a homogeneous half-space is given by (Spies and Frischknecht, 1991)

$$e_x(t) = \frac{1}{2\pi\sigma r^3} \left[\operatorname{erf}(\theta r) - \frac{2}{\sqrt{\pi}} \theta r \exp(-\theta^2 r^2) \right], \quad (7)$$

where

$$\theta = \sqrt{\frac{\sigma\mu_0}{4t}},$$

σ is the conductivity of the homogeneous half-space, r is the distance between source and receiver and $\operatorname{erf}(\cdot)$ denotes the error function.

Using an asymptotic expression of the error function for the early time $t \rightarrow 0$, one can get the early-time step-off response

$$e_x(0) = \frac{1}{\pi\sigma r^3}. \quad (8)$$

Then the normalized (dimensionless) step-off response is given by

$$\frac{e_x(t)}{e_x(0)} = \frac{1}{2} \operatorname{erf}(\theta r) - \frac{\theta r}{\sqrt{\pi}} \exp(-\theta^2 r^2). \quad (9)$$

Fig. 2.1 shows normalized step-off transient responses for a homogeneous half-space with resistivities of 0.1, 0.3, 1, 3 and 10 Ω -m. Both the transmitter and receiver exist at the surface of the half-space and the offset is 1000 m. The solid lines indicate the analytic solution given in equation (9), and the dots

represent the results from the 1-D code described above. The agreement is fairly good.

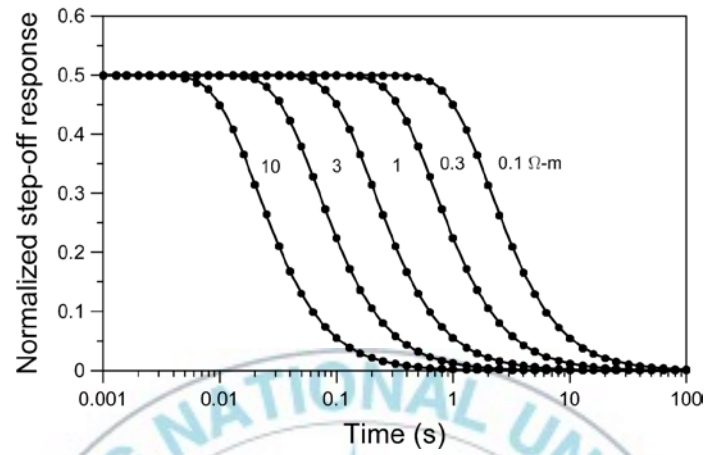


Fig. 2.1. Normalized step-off responses at the surface of the homogeneous half-space. Solid lines indicate the analytic solution and dots are numerical results from a digital filter.

Chapter 3. Marine CSEM sounding for detecting a gas-hydrate layer in the shallow seabed

3.1. Marine CSEM sounding

The basis of marine CSEM is the use of a mobile horizontal electric dipole (HED) source and an array of electric- and magnetic-field receivers on the seafloor (Fig. 3.1; Weitemeyer et al., 2006). The transmitter generates a low-frequency (typically a few to a few hundreds of Hz) EM field, which propagates both upwards in the seawater and downward within the sub-seafloor. The rate of decay in amplitude and the phase shift of the signal are controlled by both geometric and skin depth effects (Constable and Srnka, 2007). Because in general the seabed is more resistive than seawater, skin depths in the seabed are longer. As a result, EM fields at a sufficient source-receiver distance are dominated by energy propagating through the seabed. HED can excite both vertical and horizontal current flow in the seabed, maximizing resolution for a variety of structures (e.g., Constable and Srnka, 2007).

Transmitted EM signals are directly proportional to the source dipole moment, in turn given by the dipole length times the emission current. Data for interpretation are normalized by the dipole moment, so the system noise floor gets lower as the moment gets larger, allowing larger source-receiver offsets to be recorded and deeper structure to be detected. Dipole lengths are typically 100 – 300 m (Constable, 2006); making them significantly longer than that would make towing transmitter dipole close to the seafloor a technologically challenging proposition. Electric field measurements are made across electrodes mounted at the ends of plastic arms about 10 m across (Constable, 2006).

Using a 3-D modeling algorithm, Weiss and Constable (2006) demonstrated that if both source and receivers are over a tabular 3-D resistive target, 1-D modeling predicts the observed response to very high accuracy. Experimental design can thus be based on 1-D analysis to find the optimal survey parameters for a given target structure (Weitemeyer et al., 2006; Kang et al., 2010).

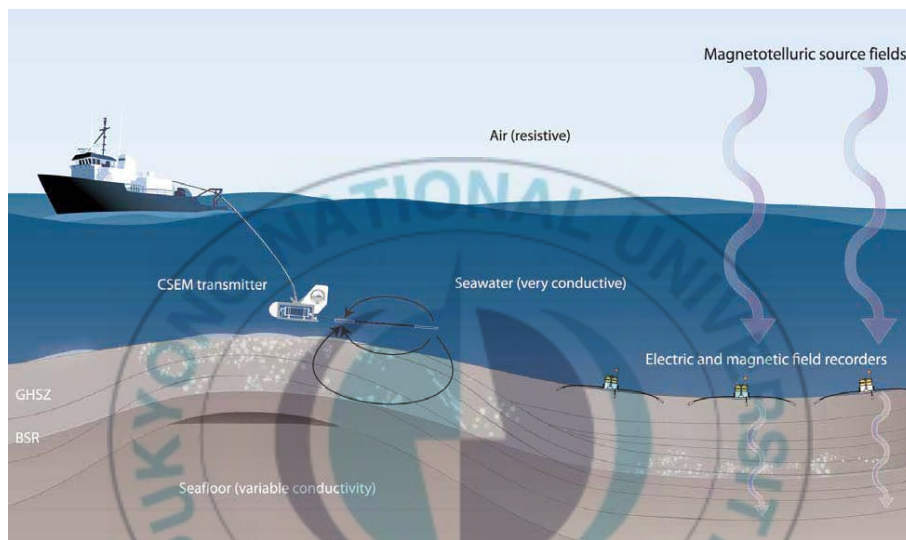


Fig. 3.1. An electric dipole transmitter is towed above the seafloor (~100 m) and an alternating EM field is transmitted along the antenna, which can be 100 – 300 m long. Seafloor receivers record electric fields (and magnetic fields) from the transmitter. BSR = bottom simulating reflector; GHSZ = gas hydrate stability zone (After Weitemeyer et al., 2006).

3.2. A gas-hydrate model

The detection capability of a gas hydrate layer depends on the frequency used and the source-receiver separation. Fig. 3.2 shows a typical 1-D marine CSEM model where the target layer is buried below the seafloor with varying depth of burial. This model is chosen on the basis of well logs gathered during ODP Leg 204 (Tréhu et al., 2006). We first consider a 1000-m seawater depth and BSR at a depth of 150 m below the seafloor. A 100 m-thick hydrate layer with a resistivity of $2 \Omega\text{-m}$ is buried in a $1 \Omega\text{-m}$ background sediment. A finite-length HED source is towed at variable height above the seafloor.

In this study we use normalized amplitude and amplitude difference simultaneously in determining the detection capability of the hydrate layer. The normalized amplitude is the field amplitude of a hydrate model response normalized by that of the model without the hydrate layer, the background model (Eidesmo et al., 2002), while the amplitude difference is the difference in amplitude between responses of the hydrate and background models (Kong et al., 2008).

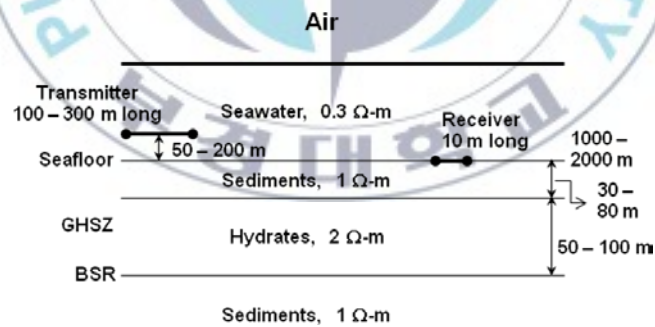


Fig. 3.2. 1-D marine CSEM model with variable depth to a resistive hydrate layer, and source length and altitude above the seafloor. EM fields are calculated for the model as a function of the transmitter-receiver separation and frequency.

EM fields from a transmitter decay rapidly, a combination of $1/r^3$ dipole geometry (r : transmitter-receiver distance) and exponential inductive attenuation. Because CSEM field amplitudes ($\text{VA}^{-1}\text{m}^{-2}$) vary over such a large range, it is useful to consider fields normalized by a background response, which is produced in the absence of the hydrate layer. The reasoning behind the employment of normalized amplitude for the analysis is that the larger it gets the easier one can differentiate the model from the background model. At the same time though, one should remember that the voltage signal must be larger than a threshold before a marine CSEM system can read it. This limit is on the order of $10^{-15} \text{VA}^{-1}\text{m}^{-2}$ (Constable and Srnka, 2007). The normalized amplitude can be numerically very large on the computer, but if the amplitudes of electric fields are smaller than the threshold, it cannot even be measured and therefore is useless.

3.3. Effect of seawater thickness

The target structure is seen over a limited range of frequency and source–receiver offset in the radial mode obtained from the in-line geometry as shown in Fig. 3.3. Frequencies below 10 Hz do not produce large effects because there is little induction in the target layer, and large electric fields are dominated by the water and sediment. At frequencies above 1000 Hz, skin depth in the sediment is only 16 m, and most energy is absorbed in the seawater and overburden. An effect of air waves is only recognized in an offset range longer than 3500 m in normalized amplitude, in which electric fields are below the current instrument system noise floor. The air wave effect disappears if the water depth is increased to 2000 m as in Fig. 3.4. In contrast, the air wave effect is almost absent in amplitude difference (compare Figs. 3.3 and 3.4). This is one of the reasons of using amplitude difference as a hydrate detection capability.

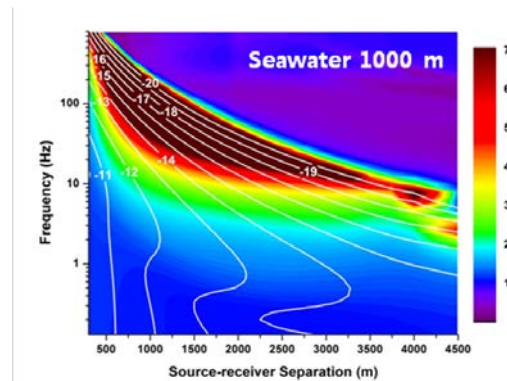


Fig. 3.3 Normalized amplitude (in color shade) and amplitude difference (in line contour, $\text{VA}^{-1}\text{m}^{-2}$) in radial mode for the hydrate model in Fig. 3.2. The hydrate layer is buried at a depth of 50 m. The source dipole length is 100 m and its altitude is 100 m above the seafloor.

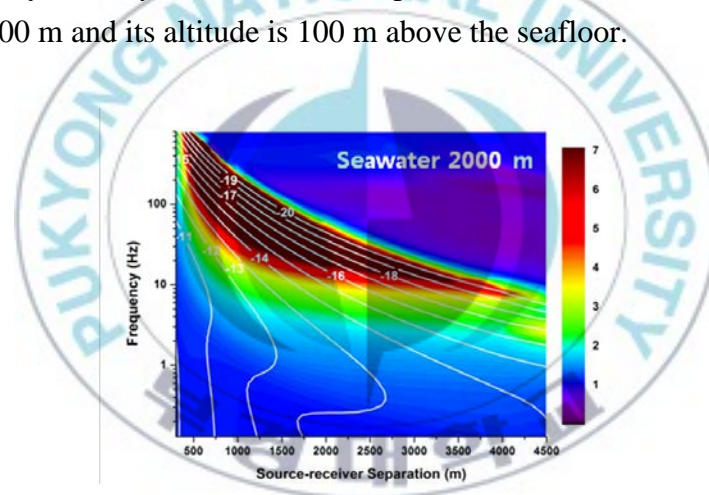


Fig. 3.4. Same as in Fig. 3.3 except that the water depth is 2000 m.

3.4. Effect of source dipole length

As mentioned above, data which show large normalized amplitudes are useful for detecting gas hydrates, provided that the actual amplitude of the field data is better than the noise threshold. Equally important, as we will find out in

a moment, is the amplitude difference. Normalized amplitudes are hardly greater than 2.0 at frequencies below 10 Hz but amplitude differences are larger than $10^{-15} \text{ VA}^{-1}\text{m}^{-2}$, which is above the noise floor, at offsets shorter than 2000 m (Fig. 3.3). These differences are on the order of a few parts per thousand of actual field amplitudes, the reason why one cannot easily tell the difference between them graphically, but can be useful data for extracting information about the hydrate layer, although this would of course require accurate data acquisition. Because the useful anomalies can be obtained at shorter offsets, it may be dangerous if we ignore the effect of dipole length.

The normalized response in Fig. 3.3 is quite similar to that obtained from a point source response (e.g., Weitemeyer et al., 2006; Kang et al., 2010). This means that the effect of dipole length is neglected almost completely if we use the normalized amplitude in the model study. If the effect of dipole length is ignored from a background half-space model, to which real field data are normalized, however, the thickness of the hydrate layer may be overestimated because elevated electric-field responses especially at short offsets persist indefinitely off the upper boundary of the target layer. Fig. 3.5 shows the effect of dipole length on the normalized amplitude and the amplitude difference. The target signal is distorted compared with Fig. 3.3 especially at higher frequencies and longer dipoles.

3.5. Comparison of electric and magnetic fields

Comparing Fig. 3.6 to Fig. 3.3, we can find that a magnetic field anomaly in terms of the normalized amplitude is quite similar to the electric field anomaly for the same model. Because magnetic field measurements are made using an induction coil in the form of dB/dt , the voltage conversion is given by

$$V \text{ in Volt} = \omega \times \text{magnetic field in } \gamma (= \text{nT}) \times 10^{-9}$$

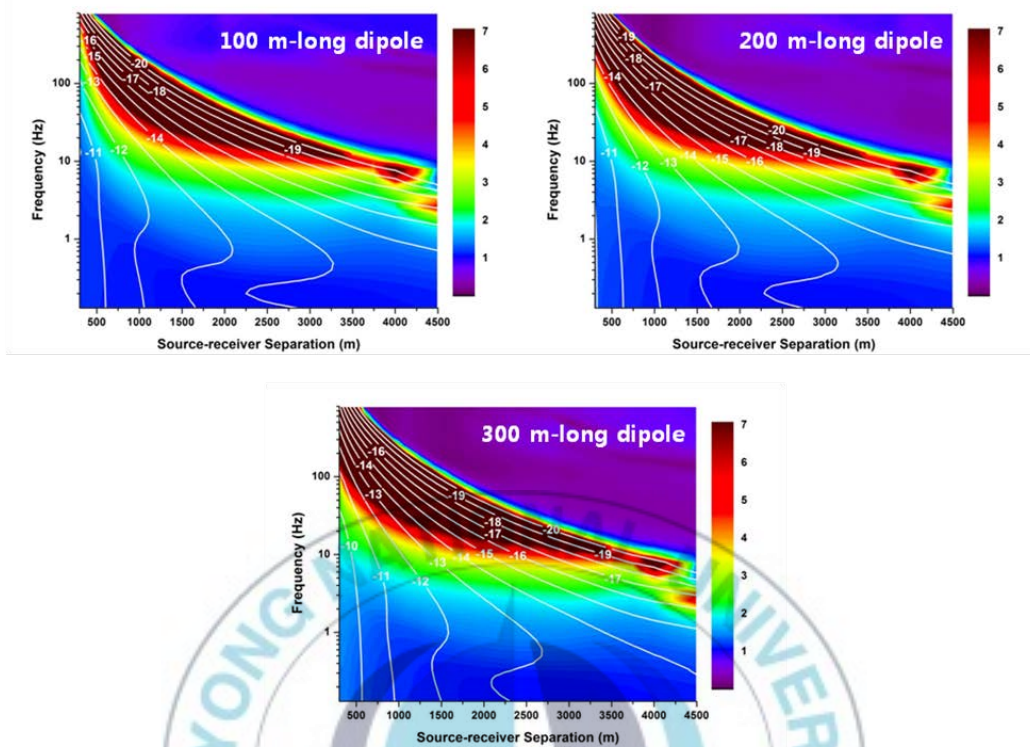


Fig. 3.5. Same as in Fig. 3.3 except that the background model is excited by a point dipole source. Three source dipole lengths are considered: (a) 100 m, (b) 200 m, and (c) 300 m.

So, a magnetic field of 10^{-7} at 10 Hz is equivalent to 2×10^{-15} V, assuming that the effective moment of receiver coil is unity. This is well above the electric field noise floor. Magnetic field measurements are made in marine CSEM methods, but motion of the sensors as water currents move the receiver instrument limits the noise floor (Constable and Srnka, 2007).

3.6. Comparison of in-line and broadside arrays

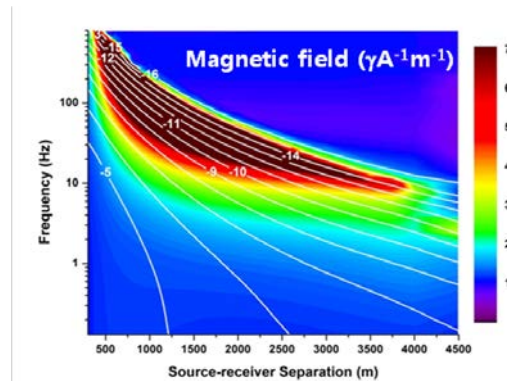


Fig. 3.6. Normalized amplitude (in color shade) and amplitude difference (in line contour) in magnetic fields ($\gamma A^{-1} m^{-1}$) for the hydrate model in Fig. 3.2. The hydrate layer is buried at a depth of 50 m. A 100 m-long dipole source is situated at 100 m above the seafloor.

Much has been made of the different behavior of the radial and azimuthal modes in the case of a deep thin resistor (e.g., Constable and Weiss, 2006), whereby the radial mode has a larger oil reservoir response than the azimuthal mode. Constable and Srnka (2007) explained this different behavior at relatively low frequencies that CSEM fields are dominated by the galvanic response of the reservoir, i.e., charge accumulation on the surface of the resistive layer associated with vertical current flow from the transmitter in the radial mode, which is largely absent in the azimuthal mode. In contrast, inductive effects dominate in the azimuthal fields and the observed response can in general be explained in terms of attenuative effects governed by EM skin depth.

When the frequency is high enough, inductive effects in the hydrate layer produce a significant response in the azimuthal mode obtained from the broadside geometry as shown in Fig. 3.7. The reduced signal below 100 Hz

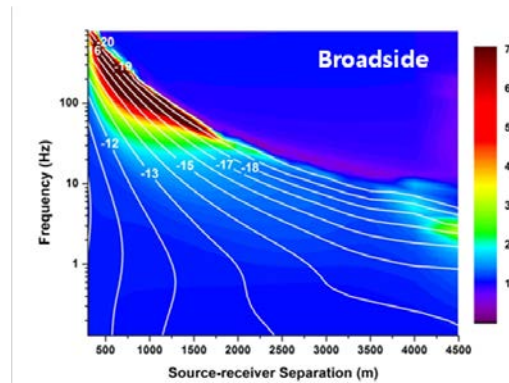


Fig. 3.7. Normalized amplitude (in color shade) and amplitude difference (in line contour, $\text{VA}^{-1}\text{m}^{-2}$) in azimuthal mode for the hydrate model in Fig. 3.2. The hydrate layer is buried at a depth of 50 m. A 100 m-long dipole source is situated at 100 m above the seafloor.

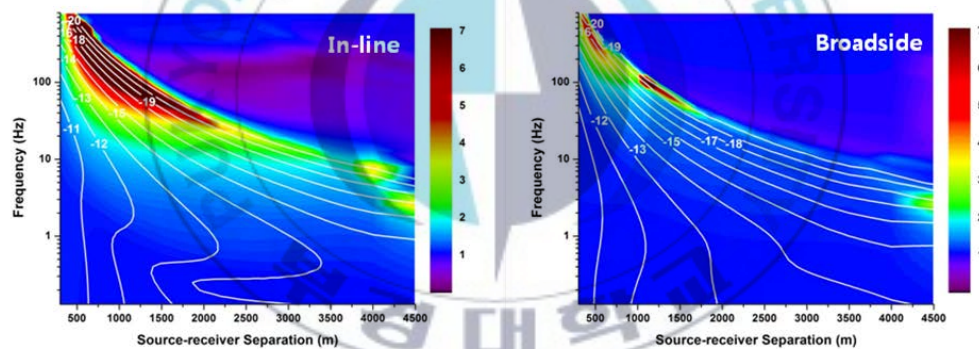


Fig. 3.8. Normalized amplitude (in color shade) and amplitude difference (in line contour, $\text{VA}^{-1}\text{m}^{-2}$) in azimuthal mode for a model with a 50 m-thick hydrate layer. The hydrate layer is buried at a depth of 50 m. A 100 m-long dipole source is situated at 100 m above the seafloor.

compared with the radial fields in Fig. 3.3 is presumably associated with the lack of galvanic contribution of the hydrate layer to the azimuthal fields. Fig.

3.8 shows inline and broadside responses for a model with a 50 m-thick hydrate layer. The hydrate signal decreases because the volume of the hydrate layer is half of the original model (100 m-thick hydrate layer) resulting in the reduction of inductive effects significantly.

3.7. Effect of source altitude

In many recent survey cruises, the transmitter is towed less than 50 m above the seafloor (e.g., Johansen et al., 2005; MacGregor et al., 2006). As we would expect, the towing altitude of the HED source has a significant effect on the target signal.

Comparing Fig. 3.9 to Fig. 3.3, we can see larger signals especially at higher frequencies as the transmitter is lowered. At low frequencies less than 10 Hz, however, the region of amplitude differences more than $10^{-15} \text{ VA}^{-1}\text{m}^{-2}$ is almost invariant to the source altitude.

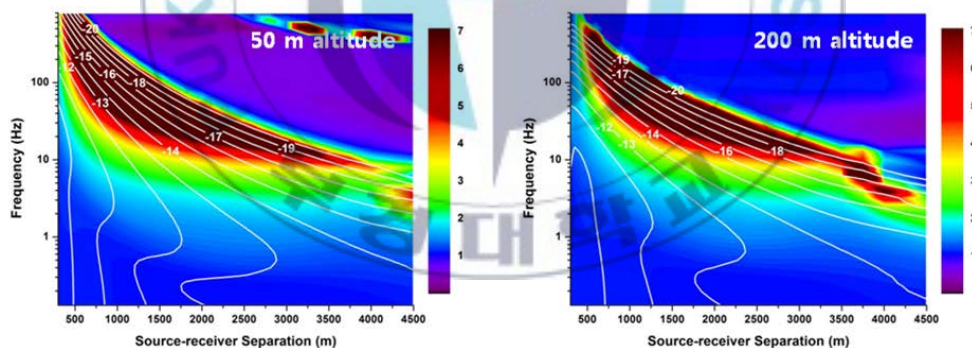


Fig. 3.9. Normalized amplitude (in color shade) and amplitude difference (in line contour, $\text{VA}^{-1}\text{m}^{-2}$) for the hydrate model in Fig. 3.2. The hydrate layer is buried at a depth of 50 m. A 100 m-long dipole source is situated at 50 m (left) and 200 m (right) above the seafloor.

3.8. Effect of overburden thickness

Since the base of HSZ is generally identified in a seismic section by the occurrence of BSR, it is important to determine the diffuse upper boundary for evaluating the total mass of hydrate. As expected, the target signal is enhanced as the burial depth becomes shallow and vice versa (Fig. 3.10). Note that if BSR is formed at a deeper place than the hydrate model in Fig. 3.2, and so the thickness of the hydrate layer is increased, the hydrate signal would be also enhanced as shown in Weitemeyer et al. (2006, Fig. 3.3).

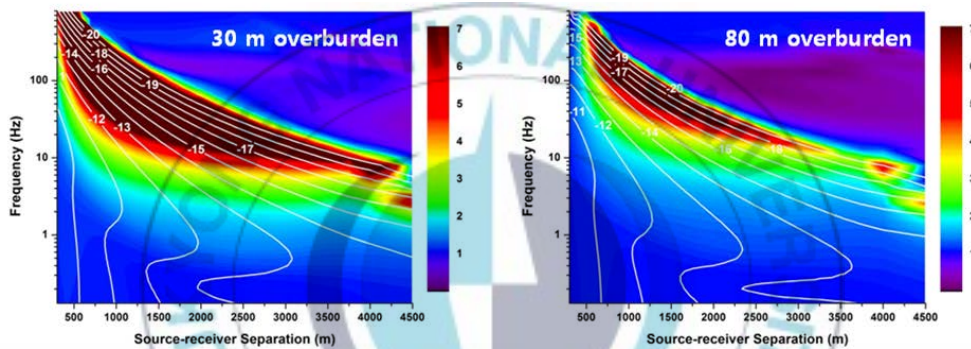


Fig. 3.10. Normalized amplitude (in color shade) and amplitude difference (in line contour, $\text{VA}^{-1}\text{m}^{-2}$) for the hydrate model in Fig. 3.2. The hydrate layer is buried at depths of 30 m (left) and 80 m (right). A 100 m-long dipole source is situated at 100 m above the seafloor.

Chapter 4. Step-off, vertical EM responses of a deep resistivity layer buried in marine sediments

4.1. Canonical reservoir model

We consider a 1-D offshore HC reservoir model shown in Fig. 4.1, which consists of $0.3 \Omega\text{-m}$ seawater with variable depth H_w , $1 \Omega\text{-m}$ seafloor sediments, and a 100 m thick, $100 \Omega\text{-m}$ HC layer at a depth of H_s below the seafloor. A 10 m -long, vertical receiver and a vertical transmitter with length L are located on the seafloor and the horizontal offset is D . In this study, the ramp time is set to be negligibly small.

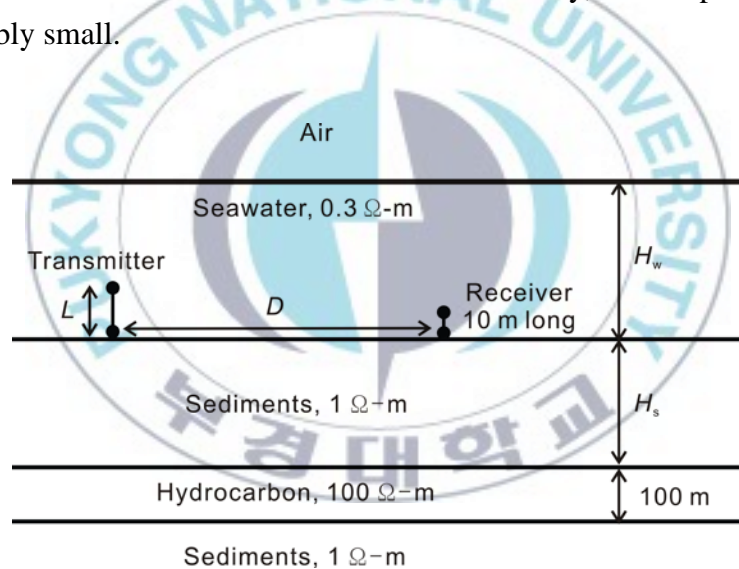


Fig. 4.1. A 1-D offshore HC reservoir model.

4.2. Comparison of electric and magnetic fields

The curves shown in Fig. 4.2 represent step-off responses of vertical electric fields for the HC reservoir model shown in Fig. 4.1 and a background two-layered model without the HC layer. The water thickness, reservoir depth and transmitter length are $H_w = 1000$ m, $H_s = 1000$ m and $L = 100$ m, respectively. The transmitter-receiver offset is $D = 500$ m. The electric field ($\text{VA}^{-2}\text{m}^{-1}$) is normalized with the source-dipole moment to make the strength of the electric field independent of the dipole length. In the illustration, absolute values of the vertical electric field are plotted, and one can see that a sign reversal of the electric field occurs at about 0.05 s.

Step-off responses are mainly galvanic at early times due to the initial current distribution, while an inductive effect dominates at late times due to the decay of induced currents. At late times t , the vertical electric field decays as $e_z(t) \sim t^{-5/2}$ in a homogeneous half-space (Ward and Hohmann, 1987). If a more resistive layer exists such as in Fig. 4.1, however, the vertical current density decays faster in time (compare the red line with the blue line in Fig. 4.2). One can see a clear anomaly compared to the response for the background model without the HC layer. In practice, the difference between the two curves is recognizable at 1 – 200 s, and the maximum contrast of more than an order of magnitude occurs at 6 s (see the gray line in Fig. 4.2) at which the electric field is well above the current instrument system noise floor, $10^{-15} \text{ VA}^{-1}\text{m}^{-2}$ (Constable and Srnka, 2007, Myer et al., 2010).

For comparison, in-line horizontal responses from a horizontal transmitter located at 50 m above the seafloor are superimposed in Fig. 4.2. The horizontal electric field is one (early times) ~ two or three (late times) orders of magnitude larger than the vertical electric field. In the case of the horizontal electric field, a sign reversal does not occur unlike the vertical one, and the sensitivity to the HC-layer is quite small at such a short offset. The sensitivity in the horizontal system will increase at longer offsets as indicated in Li and Constable (2010).

Fig. 4.3 represents step-off, horizontal magnetic-field responses at the seafloor for the HC reservoir and background models. The magnetic field also shows no sign reversal as it does in the horizontal electric field. Except at early times, however, the magnetic-field curve is quite similar in shape to the vertical electric-field curve. The magnetic field also converges to a $t^{-5/2}$ response at later times. The difference between the two magnetic-field curves is recognizable at 1 – 200 s, and the maximum contrast of more than an order of magnitude occurs at 6 s at which the magnetic field is well above the system noise floor, $10^{-18} \text{ TA}^{-1}\text{m}^{-1}$ (Myer et al., 2010, Connell and Key, 2012). Magnetic-field measurements are made also in marine CSEM methods, but motion of the sensors as water currents move the receiver instrument limits the noise floor (Constable and Srnka, 2007).

4.3. Effect of source-receiver distance

Fig. 4.4 shows step-off responses for four source-receiver distances: $D = 250, 500, 1000$ and 2000 m. In the models, H_w, H_s and L are set to 1000 m, 1000 m and 100 m, respectively. The solid lines indicate the responses over the reservoir model with the HC layer, while the dashed lines are related to the background model without the HC layer (the water-filled reservoir model). At early times, the magnitude of electric fields decreases as an increase of the offset distance. At late times, however, all curves converge to corresponding step-off responses for either the HC- or water-filled reservoir model. The maximum contrast between the responses for the two models decreases only slightly with increasing offset distance, whereas the time of sign reversal in the electric field delays significantly, suggesting that the optimal offset is less than 2000 m for the HC reservoir model.

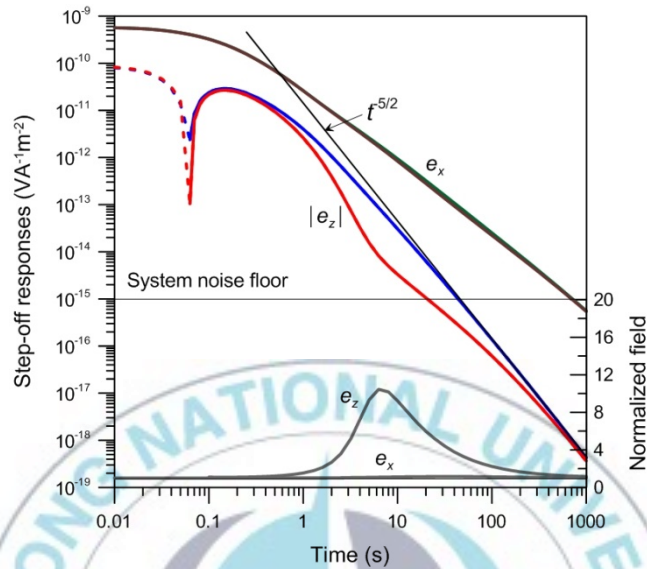


Fig. 4.2. Vertical responses from a vertical source for the HC reservoir model (red line), and the background model (blue line), and the horizontal responses from a horizontal source for the HC reservoir model (brown line) and the background model (green line). Dashed and solid lines indicate negative and positive values of the response, respectively. The bottom lines indicate the electric-field amplitudes for the HC reservoir model normalized by the responses of the background model. A 10 m-long receiver is located 500 m away from a 100 m-long transmitter at the seafloor with a water depth of 1000 m. The resistive HC layer is buried at 1000 m below the seafloor.

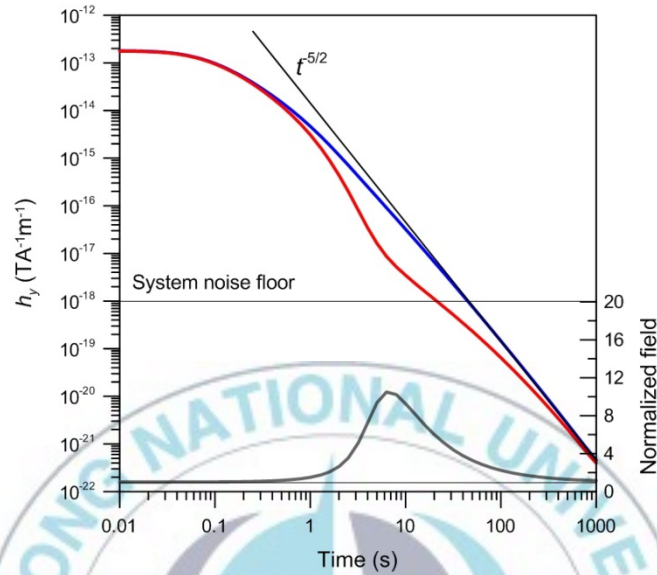


Fig. 4.3. Step-off magnetic-field responses for the HC reservoir model (red line) and the background model (blue line). The bottom gray line indicates the magnetic-field amplitude for the HC reservoir model normalized by the response of the background model. A horizontal magnetometer is located 500 m away from a 100 m-long transmitter at the seafloor with a water depth of 1000 m. The resistive HC layer is buried at 1000 m below the seafloor.

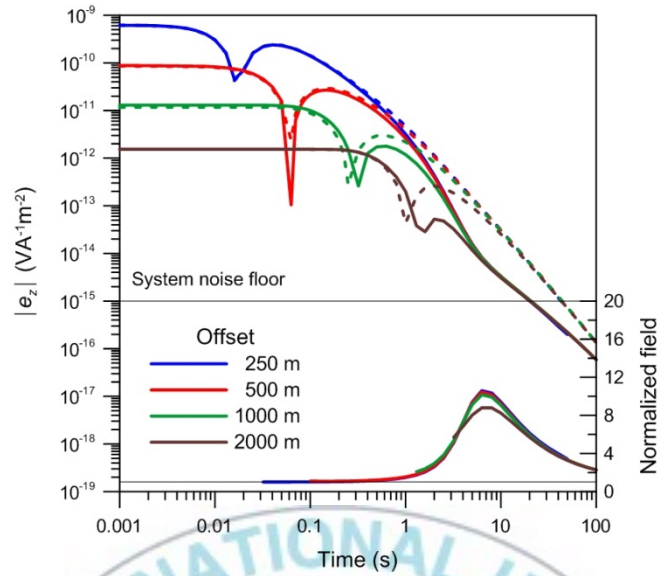


Fig. 4.4. Step-off responses for various offsets between the source and receiver over the HC reservoir model (solid lines) and the background model (dashed lines). The bottom lines indicate the ratios between the responses of the HC reservoir and the background models. A 100 m-long transmitter and 10 m-long receiver are located on the seafloor with a water depth of 1000 m. The resistive HC layer is buried at 1000 m below the seafloor.

4.4. Effect of seawater thickness

In Fig. 4.5, we compare step-off responses for three depths of water: $H_w = 500, 1000$ and 2000 m. In the models, H_s, L and D are 1000 m, 100 m and 500 m, respectively. As the sea water becomes shallow, the magnitude of electric fields decreases more rapidly at late times. The maximum contrast between the two model responses appears at $4, 6$ and 16 s when $H_w = 500, 1000$ and 2000 m, respectively, and decreases as the depth of water increases. This result shows that the vertical-vertical CSEM method can be applied in shallow water

areas, although the signal approaches faster in time to the system noise floor with decreasing depth of water. In addition, noise associated with magnetotelluric signals is greater in shallow water so that the signal-to-noise (S/N) ratio would not be very high.

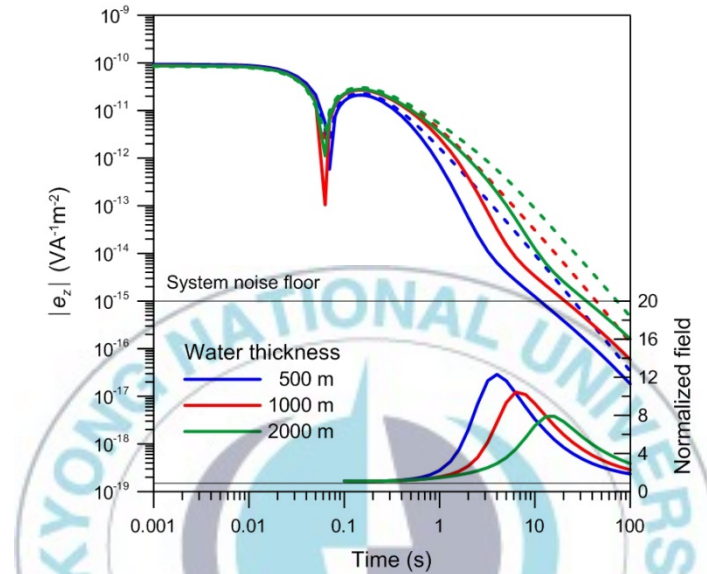


Fig. 4.5. Step-off responses for various water depths over the HC reservoir model (solid lines) and the background model (dashed lines). The bottom lines indicate the ratios between the responses of the HC reservoir and the background models. A 100 m-long transmitter and 10 m-long receiver are located on the seafloor and the offset is 500 m. The resistive HC layer is buried at 1000 m below the seafloor.

4.5. Effect of overburden thickness

Next, we examine the effect of burial depths of the resistive HC layer as shown in Fig. 4.6. Three depths of the HC layer are considered: $H_s = 500, 1000$ and 2000 m. As the burial depth of the resistive layer becomes shallow, the

magnitude of electric fields decreases more rapidly and the maximum contrast increases and appears at a faster time (4, 6, and 16 s for $H_s = 500, 1000,$ and 2000 m, respectively). In the case of $H_s = 2000$ m, the maximum contrast occurs in close proximity of the system noise floor of about 20 s. The three step-off responses eventually fall together at late times (> 20 s).

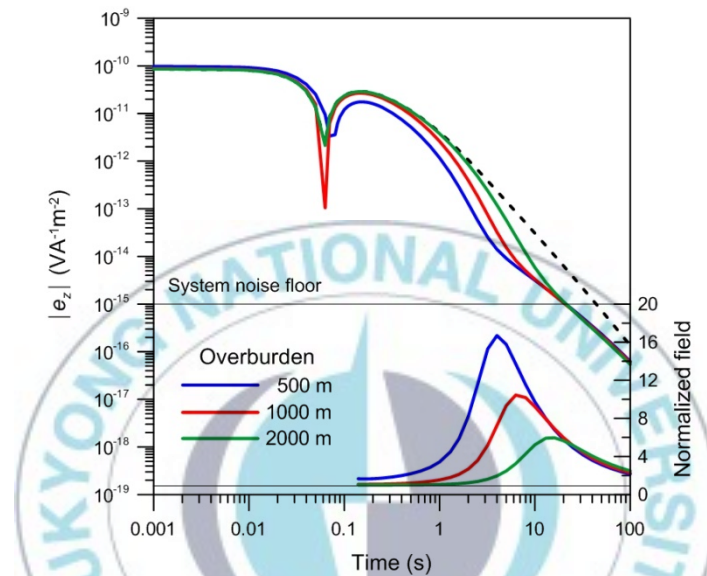


Fig. 4.6. Step-off responses for various depths of the resistive HC layer over the HC reservoir model (solid lines) and the background model (dashed line). The bottom lines indicate the ratios between the responses of the HC reservoir and the background models. A 10 m-long receiver is located 500 m away from a 100 m-long transmitter on the seafloor with a water depth of 1000 m.

4.6. Effect of source dipole length

Finally, Fig. 4.7 shows step-off responses for three lengths of the source dipole: $L = 100, 200$ and 400 m. Because the step-off response is normalized

with the source-dipole moment, it should be independent of L if the transmitter is not too long compared with the transmitter-receiver offset. When $L = 400$ m, however, one can see that the effect of the source length cannot be ignored especially at early times. The magnitude is about half of that in $L = 100$ m at 0.01 s. Through several numerical experiments, we empirically found that a point-source response is almost identical to an elongated-source response when $L/D < 0.5$, and the difference is as small as 10 %.

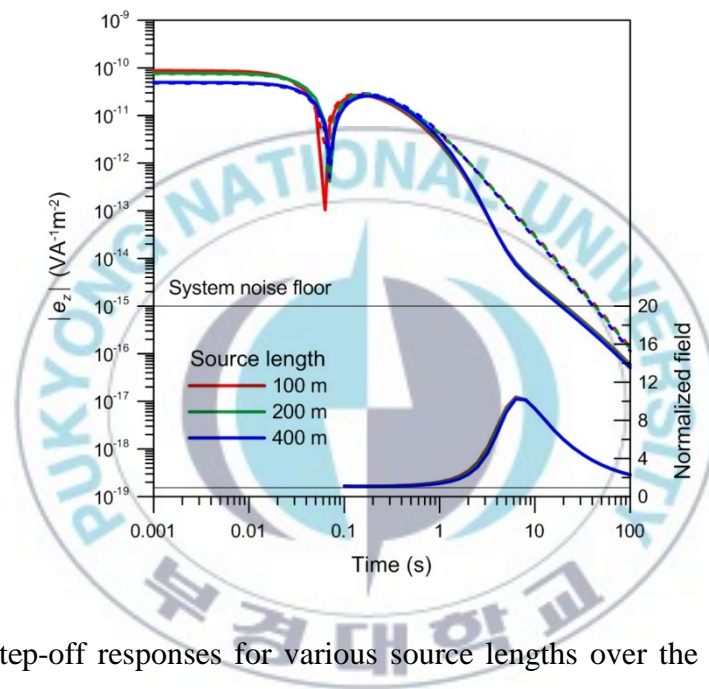


Fig. 4.7. Step-off responses for various source lengths over the HC reservoir model (solid lines) and the background model (dashed lines). The bottom lines indicate the ratios between the responses of the HC reservoir and the background models. A 10 m-long receiver is located 500 m away from the transmitter on the seafloor with a water depth of 1000 m. The resistive HC layer is buried at 1000 m below the seafloor.

Chapter 5. Discussion and conclusions

Marine CSEM methods have become an important and valuable tool in the detection of offshore hydrocarbon targets. Oil, gas and gas hydrate increase the formation resistivity of a sediment layer if they form in sufficient quantity to block previously interconnected pore space. Simple 1-D modeling is an efficient way to establish the optimum frequency and obtain an indication of the likely source-receiver offsets necessary to detect HC targets (Constable and Weiss, 2006, Connell and Key, 2012). In this study, using the frequency-domain code (Lee et al., 2011), we conducted numerical analysis to design optimum field system parameters for detecting a gas hydrate layer in the shallow section.

In this study we used normalized amplitude and amplitude difference of EM fields simultaneously in determining the detection capability of the hydrate layer. The normalized amplitude can be numerically large, but care should be taken to make sure whether or not the field can actually be measured. A large normalized amplitude is detectable at high frequencies more than 10 Hz and short offsets less than 2000 m. These frequencies and offsets will be best to distinguish the top of hydrate. At the same time, we can find that there are plenty of useful offset ranges and frequencies where amplitude difference is large enough to detect the hydrate layer. Furthermore, an effect of air waves is almost absent in amplitude difference.

Because the useful hydrate signal can be obtained at short offsets, it may be dangerous to ignore the effect of dipole length. When a point source is used for a background model, to which real field data are normalized, the target signal is distorted especially at higher frequencies and longer dipoles as shown in Fig. 3.5. As a result, the thickness of the hydrate layer would be overestimated because elevated electric-field responses especially at short offsets persist indefinitely off the upper boundary of the target layer. In

addition, navigation plays a key component in gas-hydrate detection because navigation errors are more significant at short offsets than at long ranges (Weitemeyer et al., 2006). In contrast, the adverse effect of air waves in marine CSEM data, as has been widely recognized in the oil exploration, can be avoided by acquiring data at shorter offsets.

In the case of a deep thin resistive body, the radial mode has a larger response than the azimuthal mode (Eidesmo et al., 2002; Constable and Weiss, 2006). This occurs at relatively low frequencies in which CSEM fields are dominated by the galvanic response of the oil reservoir generated by the vertical currents of the radial mode. In the case of a shallow resistive body, however, the frequency used is high enough that inductive effects in the hydrate layer produce a significant response in the azimuthal mode as shown in Fig. 3.7. In the radial mode, we can expect galvanic effects at relatively low frequencies so that the radial fields are larger than the azimuthal fields.

In this study, we develop a time-domain forward modeling code and discuss the properties of a time-domain marine CSEM method with vertical transmitters and receivers through 1-D forward modeling. The time-domain EM responses can be efficiently computed by a spline interpolation and a fast Fourier transform of the frequency-domain EM responses with multiple source and receiver dipoles that are finite in length (Lee et al., 2011).

A form of depth sounding can be made utilizing time-domain marine CSEM. In the approach with vertical transmitters and receivers, only short offsets of transmitter and receiver are necessary as shown in Fig. 4.4 and the array therefore crosses a minimum of geological boundaries such as faults and lithological contacts. In contrast, the technique with horizontal transmitters and receivers are much more affected by near-seafloor conductivity inhomogeneities since long arrays are required. Furthermore, vertical receivers are more sensitive to the edges of a sub-seafloor resistor in comparison to CSEM with horizontal receivers (Constable and Weiss, 2006), suggesting that measurements of the vertical electric field are more suitable for mapping the

lateral extent of a resistor than for recordings of the horizontal electric field.

While the vertical electric field has much smaller amplitude of signal than the horizontal field, vertical currents resulting from a vertical transmitter are sensitive to horizontal resistive layers, yielding a faster temporal decay of electric fields as in Fig. 4.2. The modeling shows a significant difference between step-off responses of HC- and water-filled reservoirs, and the contrast can be recognized at late times at relatively short source-receiver offsets. A maximum contrast occurs at more than 4 s (Figs. 4.5 and 4.6) at which the electric field is well above the system noise floor, $10^{-15} \text{ VA}^{-1}\text{m}^{-2}$ (Constable and Srnka, 2007). Myer et al. (2010) derived the same value from a CSEM survey where 0.75 Hz signals were stacked for 60 s.

Time-domain signals are probably measurable on the seafloor, but the S/N ratio would not be very high because noise associated with water motion and magnetotelluric signals increases with period (Constable, 2010). In the case of vertical fields, the magnetotelluric noise may be less significant since no vertical currents flow for horizontal structures, whereas the noise associated with water motion would be more important. Furthermore, the vertical antenna may be maximally coupled to horizontal water motion. In addition, a long recording window of about 200 s is required before the signal asymptotically approaches a steady state at the 500-m offset (Fig. 4.2). However, such a long trace is not practical, and the modeling shows that a short window, about 20 s, is sufficient to recover target signals which are above the noise threshold.

The lower S/N ratio results in considerable stacking times using a stationary transmitter (Connell and Key, 2012). The vertical transmitter is operated as a stationary one and is advantageous for the stacking of received signals. However, the parking of the transmitter on the seafloor would severely limit the amount of transmission locations for a given amount of ship survey time. On the other hand, the uncertainties of the location of transmitters do not lead to any time-dependent noise because the sub-seafloor response is recorded while the transmitter is turned off (Holten et al., 2009).

The time-domain method with vertical transmitters and receivers can be applied in shallow water areas. The contrast between responses of the HC reservoir and the background models increases as the sea water becomes shallow as partly shown in Fig. 4.5. In addition, acquisition with vertical transmitters and receivers eliminates airwave components from the received signal (Holten et al., 2009, Hunziker et al., 2011), which is one of the most significant challenges in shallow water.

In reality, the source dipole is not a point but has a physical extension. Because the useful HC signal can be obtained at shorter offsets, it may be dangerous if we ignore the effect of dipole length (Hunziker et al., 2011). To check how our modeling results change with an elongated source, a finite-length dipole was simulated by integration over the length of the dipole. In this study, because the step-off response is normalized with the source-dipole moment, it should be independent of the transmitter length (L) if the transmitter is not too long compared with the transmitter-receiver offset (D). In this study, we empirically found that a point-source response is almost identical to an elongated-source response when $L/D < 0.5$, and the difference is less than 10 %.

The key component of our modeling study is a solver that gives CSEM responses over a 1-D layered model. This solver is fast and thus easily employed in any standard inversion scheme. In practice, however, HC reservoirs are restricted in all their dimensions and are heterogeneous. This may necessitate evaluation of the response of realistic 3-D structures containing HC reservoirs. It is well known that smaller or larger 3-D effects are present in all EM methods, especially those relying on acquisition of the electric field. Thus, such a 3-D technique will be central in future developments.

References

- Chave, A. D., Constable, S. C., and Edwards, R. N., 1991, Electrical exploration methods for the seafloor, in Nabighian, M. N., ed., *Electromagnetic Methods in Applied Geophysics*, v. 2, Soc. Expl. Geophys., 931-966.
- Chave, A. D., and Cox, C. S., 1982, Controlled electromagnetic sources for measuring electrical conductivity beneath the oceans 1. Forward problem and model, *J. Geophys. Res.*, **87**, 5327-5338.
- Connell, D., and Key, K., 2012, A numerical comparison of time and frequency-domain marine electromagnetic methods for hydrocarbon exploration in shallow water, *Geophysical Prospecting*, **61**, doi: 10.1111/j.1365-2478.2012.01037.x (in press)
- Constable, S., 2006, Marine electromagnetic methods-A new tool for offshore exploration, *The Leading Edge*, **25**, 438-444.
- Constable, S., and Srnka, L. J., 2007, An introduction to marine controlled-source electromagnetic methods for hydrocarbon exploration, *Geophysics*, **72**, WA3-WA12.
- Constable, S., and Weiss, C. J., 2006, Mapping thin resistors and hydrocarbons with marine EM methods: Insights from 1D modeling, *Geophysics*, **71**, G43-G51.
- Constable, S., 2010, Ten years of marine CSEM for hydrocarbon exploration, *Geophysics*, **75**, A67-A81, doi: 10.1190/1.3483451
- Cox, C. S., Constable S. C., Chave A. D., and Webb, S. C., 1986, Controlled-source electromagnetic sounding of the oceanic lithosphere, *Nature*, **320**, 52-54, doi:10.1038/320052a0
- Edwards, R. N., Law, L. K., Wolfgram, P. A., Nobes, D. C., Bone, M. N., Trigg, D. F., and DeLaurier, J. M., 1985, First results of the

- MOSES experiment: Sea sediment conductivity and thickness determination, Bute Inlet, British Columbia, by magnetometric offshore electrical sounding, *Geophysics*, **50**, 153-161.
- Edwards, R. N., 1997, On the resource evaluation of marine gas hydrate deposits using sea-floor transient electric dipole-dipole methods, *Geophysics*, **62**, 63-74.
- Eidesmo, T., Ellingsrud, S., MacGregor, L. M., Constable, S., Sinha, M. C., Johansen, S., Kong, F. N., and Westerdahl, H., 2002, Sea Bed Logging (SBL), a new method for remote and direct identification of hydrocarbon filled layers in deepwater areas, *First Break*, **20**, 144-152.
- Ellingsrud, S., Eidesmo, T., Johansen, S., Sinha, M. C., MacGregor, L. M., and Constable, S., 2002, Remote sensing of HC layers by seabed logging (SBL): Results from a cruise offshore Angola, *The Leading Edge*, **21**, 972-982.
- Hunziker, J., Slob, E., and Mulder, W., 2011, Effects of the airwave in time-domain marine controlled-source electromagnetics, *Geophysics*, **76**, F251-F261, doi: 10.1190/1.3587222
- Holten, T., Flekkøy, E. G., Singer, B., Blixt, E. M., Hanssen, A., and Maløy, K. J., 2009, Vertical source, vertical receiver, electromagnetic technique for offshore hydrocarbon exploration, *First Break*, **27**, 89-93.
- Johansen, S., Amundsen, H. E. F., Rosten, T., Ellingsrud, S., Eidesmo, T., and Bhuyian, A. H., 2005, Subsurface hydrocarbons detected by electromagnetic sounding, *First Break*, **23**, 31-36.
- Kang, S., Seol, S. J., and Byun, J., 2010, An investigation in operating and design parameters for gas hydrate exploration using marine CSEM, *J. Korean Soc. Geosystem Eng.*, **47**, 139-150. (in Korean)

with English abstract)

- Kang, S., Seol, S. J., and Byun, J., 2012, A feasibility study of CO₂ sequestration monitoring using the mCSEM method at a deep brine aquifer in a shallow sea, *Geophysics*, **77**, E117-126, doi: 10.1190/geo2011-0089.1
- Kim, H. J., Song, Y., and Lee, K. H., 1997, High-frequency electromagnetic inversion for a dispersive layered earth, *J. Geomag. Geoelectr.*, **49**, 1439-1450.
- Kong, F. N., Johnstad, S. E., Røsten, T., and Westerdahl, H., 2008, A 2.5D finite-element-modeling difference method for marine CSEM modeling in stratified anisotropic media, *Geophysics*, **73**, F9-F19.
- Lee, K. H., Jang, H., Jang, H., and Kim, H. J., 2011, Sensitivity analysis of marine controlled-source electromagnetic methods to a shallow gas-hydrate layer with 1D forward modeling, *Geosciences Journal*, **15**, 297-303, doi: 10.1007/s12303-011-0030-z
- Li, Y. G., and Constable, S., 2010, Transient electromagnetic in shallow water: insights from 1D modeling, *Chinese J. Geophys.*, **53**, 737-742.
- MacGregor, L. M., Andreis, D., Tomlinson, J., and Barker, N., 2006, Controlled-source electromagnetic imaging on the Nuggets-1 reservoir, *The Leading Edge*, **25**, 984-992.
- Myer, D., Constable, S., and Key, K., 2010, A marine EM survey of the Scarborough gas field, Northwest Shelf of Australia, *First Break*, **28**, 77-82.
- Scholl, C., and Edwards, R. N., 2007, Marine downhole to seafloor dipole-dipole electromagnetic methods and the resolution of resistive targets, *Geophysics*, **72**, WA39-WA49, doi: 10.1190/1.2434775

- Schwalenberg, K., Willoughby, E., Mir, Reza, and Edwards, R. N., 2005, Marine gas hydrate electromagnetic signatures in Cascadia and their correlation with seismic blank zones, *First Break*, **23**, 57-63.
- Song, Y., Kim, H. J., and Lee, K. H., 2002, High frequency electromagnetic impedance for subsurface imaging, *Geophysics*, **67**, 501-510.
- Spies, B. R., and Frischnecht, F. C., 1991, Electromagnetic sounding, in Nabighian, M. N., ed., *Electromagnetic Methods in Applied Geophysics*, v. 2, Soc. Expl. Geophys., 285-425.
- Tr'ehu, A., Torres, M., Bohrmann, G., and Colwell, F., 2006, Leg 204 Synthesis: Gas hydrate distribution and dynamics in the Central Cascadia accretionary complex. Proc. of Ocean Drilling Program, Scientific Results, 204, 1-40.
- Um, E. S., and Alumbaugh, D. L., 2007, On the physics of the marine controlled-source electromagnetic method, *Geophysics*, **72**, WA13-WA26.
- Ward, S. H., and Hohmann, G. W., 1987, Electromagnetic theory for geophysical applications, in Nabighian, M. N., ed., *Electromagnetic Methods in Applied Geophysics*, v. 1, Soc. Expl. Geophys., 203-252.
- Weiss, C. J., and Constable, S., 2006, Mapping thin resistors and hydrocarbons with marine EM methods, Part II-Modeling and analysis in 3D, *Geophysics*, **71**, G321-G332.
- Weiss, C. J., 2007, The fallacy of the "shallow-water problem" in marine CSEM exploration, *Geophysics*, **72**, A93-A97, doi: 10.1190/1.2786868
- Weitemeyer, K., Constable, S., and Key, K., 2006, Marine EM techniques for gas-hydrate detection and hazard mitigation, *The Leading Edge*, **25**, 629-632.

- Yuan, J., and Edwards, R. N., 2000, The assessment of marine hydrates through electrical remote sounding: Hydrate without a BSR?, *Geophysical Research Letters*, **27**, 2397-2400.
- Ziolkowski, A., 2007, Developments in the transient electromagnetic method, *First Break*, **25** 99-106.



Appendix: Waveform harmonics

The step-off waveform is treated as a box-car waveform with a long on and off time. Ramp time on both sides of the on time is an option. The duration of the on time is internally determined by the last of an output time sequence, which starts ($t = 0$) at the base of off-ramp. The harmonics of the step-off waveform is

$$F_{\text{Step-off}}(\omega) = \left\{ \begin{array}{l} \frac{1}{T_r} \frac{i}{\omega} \exp[i\omega(T_r + T_{\text{on}})] \left[\frac{i}{\omega} \exp(i\omega T_r) + T_r - \frac{i}{\omega} \right] \\ + \frac{i}{\omega} \exp[i\omega(T_r + T_{\text{on}})] [\exp(-i\omega T_{\text{on}}) - 1] \\ + \frac{1}{T_r} \frac{i}{\omega} \exp(i\omega T_r) \left[\frac{i}{\omega} \exp(-i\omega T_r) - T_r - \frac{i}{\omega} \right], \omega \neq 0 \\ T_r + T_{\text{on}}, \omega = 0 \end{array} \right\}, \quad (\text{A1})$$

where T_{on} and T_r are the on time and ramp time, respectively. The on time and off time are given equal internally, and the period of this waveform is $T = T_{\text{on}} + T_{\text{off}} + 2T_r$.

A variable on and off time square wave is followed by the same sequence with reversed polarity. Ramp time is an option. As is the step-off case, output time sequence starts at the base of off-ramp. The harmonics of the square waveform can be simply constructed by combination of the step-off harmonics and its phase shifted reversed polarity component as

$$F_{\text{Square}}(\omega) = \left\{ \begin{array}{l} F_{\text{Square}}(\omega) [1 - \exp(i\omega t / 2)], \omega \neq 0 \\ 0, \omega = 0 \end{array} \right\}. \quad (\text{A2})$$

The on and off time are variable, and the period of this waveform is $T = 2(T_{\text{on}} + T_{\text{off}} + 2T_r)$.

The source is a normalized Gaussian probability function defined as

$$f(t) = \sqrt{\frac{\alpha}{\pi}} \exp(-\alpha t^2).$$

It's integral over time is unity, similar to that of the Dirac delta function. As the variable α becomes large, it gets close to the delta function. The delta-ness of the waveform is controlled by a half-width of the pulse

$$t_{\text{half-width}} = \sqrt{\frac{\log 2}{\alpha}}.$$

The smaller the half-width time, the more it becomes an impulse. An output time sequence starts at the peak of the pulse. The harmonics of the Gaussian waveform is

$$F_{\text{Gaussian}}(\omega) = \begin{cases} \exp(-\omega^2 / 4\alpha), & \omega \neq 0 \\ 1, & \omega = 0 \end{cases}. \quad (\text{A3})$$

The waveform consists of a sequence of half-sine with reversed polarity and variable off time in between. So, the period is given by $T = 2(T_{\text{on}} + T_{\text{off}})$. An output time sequence starts at the end of the positive half sine. The harmonics of the INPUT waveform is

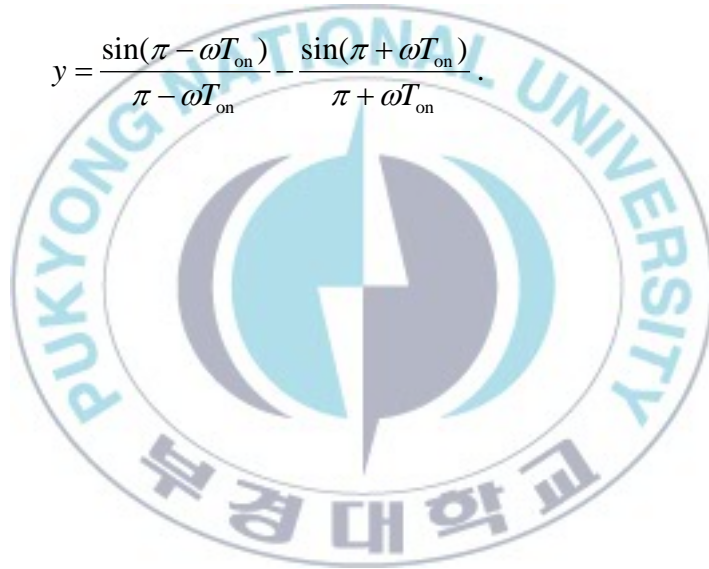
$$F_{\text{INPUT}}(\omega) = F_0(\omega) [\exp(-i\omega T) - \exp(-i\omega T / 2)], \quad (\text{A4})$$

where

$$F_{\text{INPUT}}(\omega) = \begin{cases} \frac{T_{\text{on}}}{2}(x + iy), & \omega \neq \frac{\pi}{T_{\text{on}}} \\ i \frac{T_{\text{on}}}{2}, & \omega = \frac{\pi}{T_{\text{on}}} \end{cases},$$

$$x = \frac{1 - \cos(\pi - \omega T_{\text{on}})}{\pi - \omega T_{\text{on}}} + \frac{1 - \cos(\pi + \omega T_{\text{on}})}{\pi + \omega T_{\text{on}}},$$

$$y = \frac{\sin(\pi - \omega T_{\text{on}})}{\pi - \omega T_{\text{on}}} - \frac{\sin(\pi + \omega T_{\text{on}})}{\pi + \omega T_{\text{on}}}.$$



해양자원탐사를 위한 인공송신원 전자탐사법의 모델링 연구

장한길로

부경대학교 대학원 에너지자원공학과

초 록

주파수영역 인공송신원 해양 전자탐사법은 심해의 탄화수소 저류층 탐지에 성공적으로 적용되어왔다. 하지만 수평의 송신기와 수신기를 이용하는 일반적인 방법은 목표 심도에 따라 큰 송수신 간격을 필요로 한다. 수직전기장은 깊은 저항층에 민감하기 때문에 수직의 송신기와 수신기를 이용하는 시간영역 전자탐사 시스템은 하나의 대안이 될 수 있다. 주파수영역과 시간영역에서 유한 길이의 다중 송수신 쌍극자에 의한 1차원 전자기 반응을 측정하기 위해 컴퓨터 프로그램들을 개발하였다. 주파수영역의 1차원 프로그램을 이용하여, 얇은 수심의 가스하이드레이트층에 대한 해양 전자탐사법의 감도분석을 시도해냈다. 본 연구에서는 하이드레이트층의 탐지 가능성을 결정하기 위해 전자기장의 정규화된 진폭과 진폭의 차이를 동시에 이용하였다. 반응 진폭은 하이드레이트층을 포함하지 않는 배경매질 모델로 정규화하였다. 그러나 정규화된 진폭은 수치적으로 클 수 있지만, 반응 진폭이 측정 한계치보다 작다면 이는 잘못된 결과이며 유용하지 않다. 목표층을 탐지하기에 충분히 진폭 차이가 큰 영역에서 유용한 송수신 간격들과 주파수들이 많음을 알 수 있었다. 게다가 공기파의 영향은 진폭 차이에서 거의 나타나지 않는다. 시간영역 프로그램을 이용하여, 1차원 탄화수소 저류층 모델에 대한 step-off 반응들을 계산하였다. 수직전기장은 수평전기장에 비해 신호의 크기가 작음에도 불구하고, 수직의 송신기에 의해 발생된 수직 전류는 저항층에 민감하다. 모델링 결과는 탄화수소로 가득 찬 저류층과 해수로 가득 찬 저류층 사이에서 큰 차이를 보여주며, 이러한 차이는 상대적으로 짧은 송수신 간격의 후기 시간대에서 인지 할 수 있다. 최대 차이는 4초 이후에 발생하며,

탄화수소층의 심도에 따라 그 발생시간은 지연된다.

주요어: 해양 인공송신원 전자탐사, 가스하이드레이트, 정규화된 진폭, 진폭 차이, 공기파, 탄화수소, step-off 반응, 수직 송신기



감사의 글

이번 겨울은 유난히도 추운 겨울이지만 너무나 많은 분들의 도움과 가르침이 생각나 따뜻함을 느낍니다.

가장 먼저 논문의 완성과 졸업을 할 수 있도록 사소한 부분 하나부터 모든 것을 가르쳐 주시고 지원해 주신 김희준 교수님께 감사의 말을 전합니다. 아직 너무나 부족하고 배워야 할 것이 넘치지만 부끄러운 제자가 되지 않도록 노력하겠습니다. 또한, 바쁘신 와중에도 심사를 위해 시간을 내어주시고 진심 어린 조언을 해 주신 엄정기 교수님과 최요순 교수님 그리고 에너지자원공학과와 다른 모든 교수님의 가르침으로 무사히 졸업할 수 있게 되었습니다. 감사합니다. 지금은 한국에 안 계시지만 처음으로 물리탐사에 흥미를 느끼게 해 주셨던 이기하 박사님께도 감사의 말을 전하고 싶습니다.

그리고 현장에서 하나라도 저에게 더 가르침을 전해 주려 하시는 이동성 박사님, 박미경 박사님께 감사드립니다. 저의 앞날을 진심으로 걱정해 주시며 많은 조언을 해주신 최지향 박사님께도 꼭 감사하다는 말을 하고 싶습니다. 또한, 제가 지금의 자리에 있기까지 항상 옆자리에서 저를 챙겨주시는 저의 가장 가까운 선배이자, 친구이자 때론 어머니 같은 저의 친누나 장한누리 박사님께 진심으로 감사의 인사를 전합니다. 학과 사무실의 황병준 조교님, 신선미 조교님 그리고 특성화 사무실의 김선옥 교수님, 조지현 조교님의 도움 또한 잊지 않겠습니다.

대학원 동기인 김소희, 남지은, 노영환, 모철훈, 박은두, 서현교 학생에게도 앞날에 무궁한 영광이 있기를 바라며, 언제라도 서로에게 무슨 일이 생기면 당장이라도 달려나올 수 있는 나의 최고의 보물들 나의 고등학교 친구들에게 꼭 고맙다는 말을 하고 싶습니다.

마지막으로 사랑하는 부모님, 항상 사고만 치고 말썽만 일으키는 아들이 하고 싶은 걸 하도록 묵묵히 지켜봐 주셔서 너무나 미안한 마음뿐입니다. 이 은혜 잊지 않겠습니다.